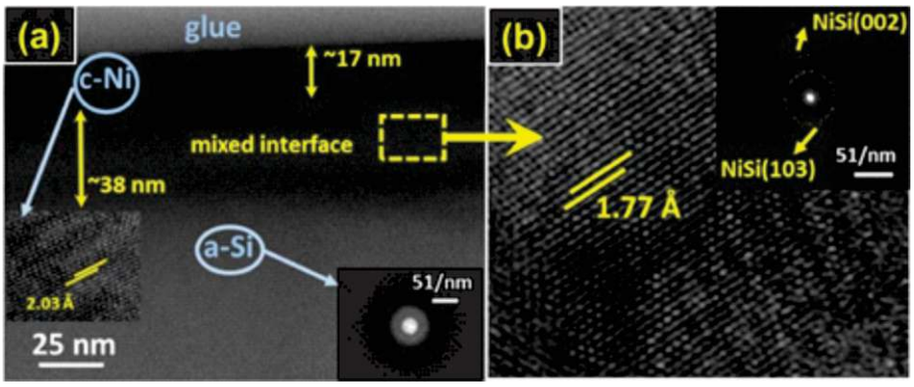


***Fig. 4.4.4.3.1.2:*** *(a) XTEM image of irradiated Ni (30 nm)/Si sample. Diffraction pattern obtained from amorphous Si region and HRTEM image obtained from unreacted c-Ni region are in insets. (b) The HRTEM image from the selected rectangular region [1].*

### 4.4.4.3.2 Study of morphological and structural properties of 2D materials

Abid et al. has studied the synthesis of mono- to few-layer $WS_2$ film on graphene-oxide (GO) coated $Si/SiO_2$ substrate using the CVD technique [2]. The uniform mono-to-few layer growth over the entire substrate has been reaffirmed by HRTEM. In Fig. 4.4.4.3.2.1(a), the hexagonal flakes have been measured to be of about ~2.5 µm. In Fig. 4.4.4.3.2.1(b), the distorted cum truncated $WS_2$ triangle has been observed clearly. At higher resolutions, in Fig. 4.4.4.3.2.1(c)-(d), the crystalline nature of the flakes has been observed. In Fig. 4.4.4.3.2.1(e), the SAED pattern has confirmed the highly crystalline morphology of as-grown $WS_2$[2].

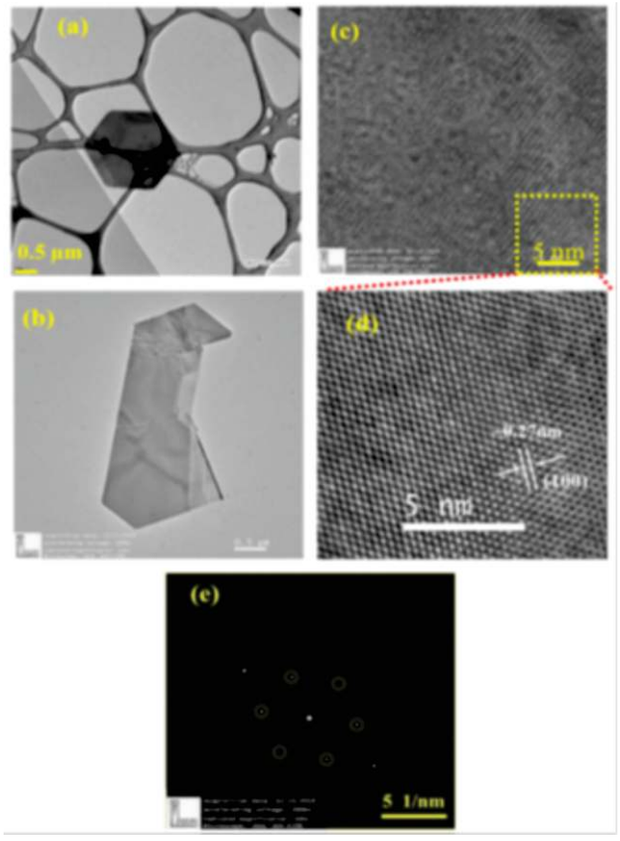


***Fig. 4.4.4.3.2.1:*** *The TEM images of $WS_2$ flakes shown in (a) and (b) at low magnification, (c) at high magnification. (d) magnified view of (c), and (e) SAED pattern of the magnified area [2].*

A two-step synthesis by a chemical route method followed by a hydrothermal technique to produce 2D/3D hybrid material has been studied by Nahid Chaudhary et al., wherein $MoS_2$ nanosheets have been integrated with the 3D cube-like network of PbS [3]. HRTEM images, in Fig. 4.4.4.3.2.2(a), show the network of interconnected nanostructure frameworks, including both $MoS_2$ NSs and PbS nanocubes, with pronounced regularity over the entire surface [3]. A single cube of PbS has been shown in Fig. 4.4.4.3.2.2(b) which shows diffused dimensions of PbS. $MoS_2$ NSs and PbS nanocubes have been identified in Fig. 4.4.4.3.2.2(c) with the lattice spacing of 0.62 nm corresponding to (002) plane of $MoS_2$ NSs and with nanocube lengths of around 70−100 nm. In Fig. 4.4.4.3.2.2(d), SAED pattern has shown the pure crystalline nature of the 2D/3D $MoS_2$/PbS hybrid structure with the diffraction planes (0111) and (006) and (200) and (311) corresponding to $MoS_2$ and PbS, respectively, and well correlated with the XRD pattern [3].

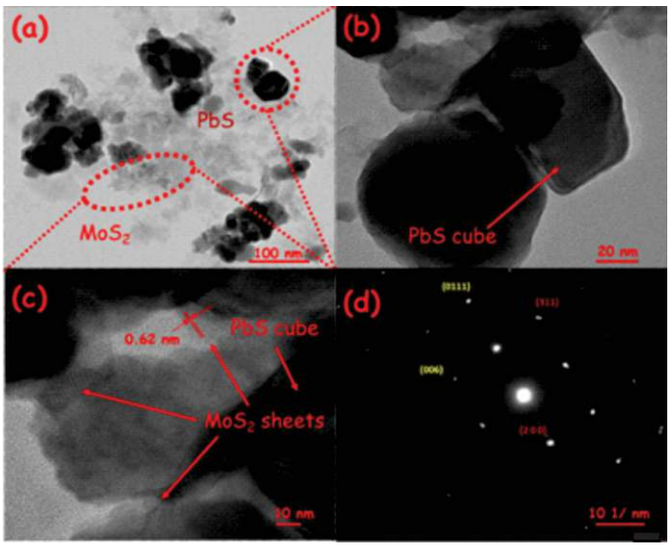


***Fig. 4.4.4.3.2.2:*** *TEM images of the (a) $MoS_2$/PbS hybrid material, (b) PbS cube, (c) $MoS_2$ NSs, and (d) SAED pattern confirming the crystalline nature of the composite material [3].*

In a similar kind of study, Dhirendra Sahoo et al. synthesized the luminescent nanocrystals $MoS_2$ by hydrothermal method [4]. In Fig. 4.4.4.3.2.3(a), the HRTEM image of $MoS_2$ nanocrystals shows that the $MoS_2$ nanocrystals of the diameters of 2–10 nm have been distributed uniformly. The size distribution of $MoS_2$ nanocrystals has been depicted in Fig. 4.4.4.3.2.3(b). The high-crystalline nature of the nanocrystals with a lattice spacing of 0.2 nm corresponding to (006) plane has been shown in Fig. 4.4.4.3.2.3(c).

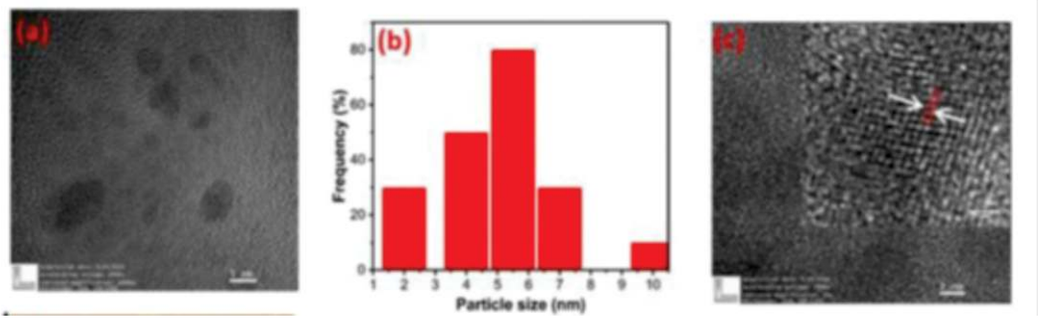


***Fig. 4.4.4.3.2.3:*** *(a) HRTEM image of $MoS_2$ nanocrystals (b) size distribution of $MoS_2$ nanocrystals (c) HRTEM image showing the lattice fringes of $MoS_2$ nanocrystals [4].*

Structural and electronic properties of few-layers $MoS_2$ film on $SiO_2$/Si substrate have been studied by Mayur Khan et al. [5]. In Fig. 4.4.4.3.2.4(a)-(b), the shown TEM and HRTEM images have been recorded from the random areas of the $MoS_2$ deposited TEM grid. The flakes of the $MoS_2$ and their stacking have been observed in the TEM image shown in Fig. 4.4.4.3.2.4(a). A few layers are grown $MoS_2$ has been shown in the HRTEM image in Fig. 4.4.4.3.2.4(b). The planes (100) and (008) have been observed in the FFT image in the inset (top right corner). The hexagonal structure of $MoS_2$ has been confirmed by the magnified image of dotted box at inset (lower left corner) [5].

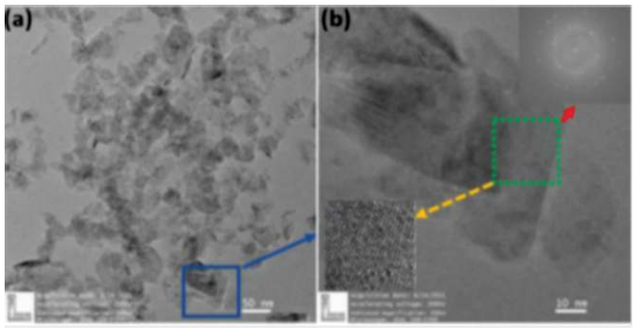


***Fig. 4.4.4.3.2.4:*** *(a) TEM and (b) HRTEM images of few-layers $MoS_2$ [5].*

### 4.4.4.3.3 Morphological and structural characterization of thin films, powder samples and embedded systems

Hemant Jatav et al. has studied the effects of metal concentration and annealing temperature on the optical properties of silver nanocomposite [6]. The HRTEM image of the as-deposited Ag-$SiO_2$ nanocomposite sample shown in Fig. 4.4.4.3.3.1(a), confirms that the Ag nanoparticles along with the unstable small clusters have been formed during the deposition [6]. The mean diameter of the spherical Ag nano-particles has been measured to be 3.03 ± 0.60 nm [6]. The average size of the Ag NPs has increased to 4.61 ± 1.49 nm with increasing the annealing temperature to 400 ˚C, as shown in Fig. 4.4.4.3.3.1(c).

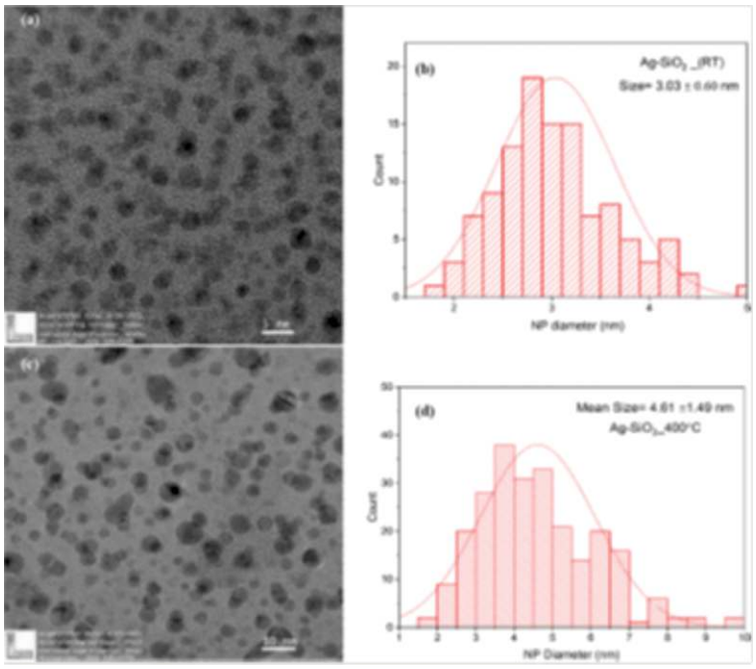


***Fig. 4.4.4.3.3.1:*** *HRTEM images of HVF Ag-$SiO_2$ nanocomposite of (a) as deposited sample and (c) annealed at 400 ˚C. NPs size distribution (b) as deposited (d) annealed at 400 ˚C samples [6].*

Ankush Saxena et al. has reported the single crystal growth of $SnSb_2Te_4$ using the self-flux method to study the structural and weak anti-localization analysis [7]. For TEM characterization, the synthesized crystal has been crushed and dispersed on the TEM grid. The crystalline nature of the synthesized $SnSb_2Te_4$ crystals has been confirmed by SAED and HRTEM images.

Afroz Khan et al. has investigated the structural, morphological, optical, and electrical properties of PLD grown high quality $In_{2-x}Sn_xO_3$ thin films on quartz substrates as a function of substrate deposition temperatures and the Sn compositions [8]. TEM characterization has been carried out to investigate the crystallinity and particle size distribution of deposited ITO films at 450 ˚C. The spherical geometry with some agglomeration of nano-crystallites for x = 0.1 and x = 0.2 has been verified by TEM images as depicted in Fig. 4.4.4.3.3.2(a) and (d), respectively. The particle size distribution along with the Gauss curve fitting, in Fig. 4.4.4.3.3.2(c) and (f), has shown the particle sizes of 63 nm and 51 nm for x = 0.1 and 0.2, respectively which has good concurrence with the results obtained from XRD analysis [8].

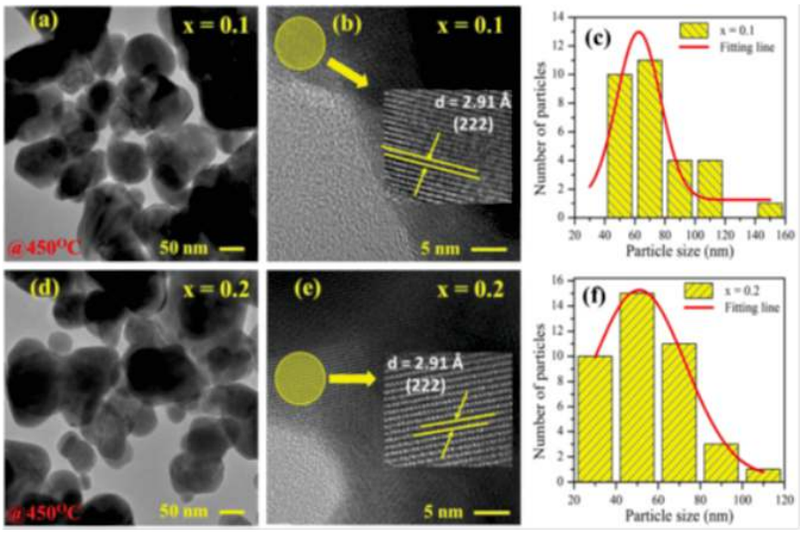


***Fig. 4.4.4.3.3.2:*** *(a) and (d) TEM images, (b) and (e) HRTEM images, enlarged area with inter-planer spacing corresponding to (222) plane in insets and particle size distributions in (c) and ( f) of $In_{2-x}Sn_xO_3$ thin films with deposition temperature 450 ˚C for x = 0.1 and x = 0.2, respectively [8].*

## References

[1] "Growth of low resistive nickel mono-silicide phase under low energy Si ion irradiation at room temperature", G. Maity, S. Ojha, G.R. Umapathy, Shiv P. Patel, Anter El Azab, Kailash Pandey, Santosh Dubey, Thin Solid Films 733 (2021) 138826

[2] "Interface Kinetics Assisted Barrier Removal in Large Area 2D-$WS_2$ Growth to Facilitate Mass Scale Device Production", Abid, Poonam Sehrawat, Christian M. Julien, Saikh S. Islam, Nanomaterials 11 (2021) 220

[3] "High-Performance Supercapacitor Electrode Material Based on the Two-Dimensional/Three-Dimensional Architecture of $MoS_2$–PbS Hybrid Material", Nahid Chaudhary, Manika Khanuja, Energy Fuels 36, 2 (2022) 1034–1042

[4] "Cost-effective synthesis of 2D molybdenum disulfide ($MoS_2$) nanocrystals: An exploration of the influence on cellular uptake, cytotoxicity, and bio-imaging", Dhirendra Sahoo, Sushreesangita P. Behera, Jyoti Shakya, Bhaskar Kaviraj, PLoS ONE 17(1) (2022) e0260955

[5] "Study of structural and electronic properties of few-layer $MoS_2$ film", Mayur Khan, Sunil Kumar, Ambuj Mishra, Indra Sulania, Madhvendra Nath Tripathi, Ambuj Tripathi, Materials Today Proceedings (article in press)

[6] "The effects of metal concentration and annealing temperature on the optical properties of silver nanocomposite", Hemant Jatav, Ambuj Mishra, D Kabiraj, Materials Today Proceedings (article in press)

[7] "Structural and weak antilocalization analysis of topological single-crystal $SnSb_2Te_4$", Ankush Saxena, M.M. Sharma, Prince Sharma, Yogesh Kumar, Poonam Rani, M. Singh, S. Patnaik, V.P.S. Awana, Journal of Alloys and Compounds 895 (2021) 162553

[8] "Role of deposition temperature and Sn content on structural, optical & electrical properties of $In_2O_3$ thin films", Afroz Khan, F. Rahman, Razia Nongjai, K. Asokan, Current Applied Physics 38 (2022) 49–58

### 4.4.5 Structure and Spectroscopy Lab

Abid Hussain, Himanshi Gupta, Vishnu K. Chauhan, Sanjay K. Kedia, and Fouran Singh

The laboratory is having several research facilities for the development and characterizations of materials namely RF sputtering, e-beam evaporator, tubular furnace, high temperature furnace, in-situ micro-Raman spectrometer, in-situ X-ray diffractometer, Uv-Vis-NIR spectrometer, FTIR, photo-luminance spectrometer, solar simulator, etc. These research facilities have been extensively used by the many researchers from Indian universities/institutes and aboard working on different types of materials. The facilities are in regular operation besides regular upkeep for research in materials science. About 550 samples have been characterized for users from different institutes/universities including both thin films and bulk samples. About 100, 496 and 341 spectra have been taken using PL, FTIR and UV-Vis-NIR facilities for various users. However, presently micro-Raman facility has been down, and efforts have been put with the support from Renishaw to make the system operational soon for regular experiments. The sputtering system has been upgraded by replacing or repairing its various components such as temperature controller, substrate rotation, PID controller, vacuum gauge, thickness monitor and water, and air pipes. It was also noted that the machine has capabilities to sputter the three targets simultaneously but only one gun is operational which limits the machine to sputter a single target. Therefore, one more gun was repaired locally and tested to enable the co-sputtering. The machine was tested to co-sputter the FeGa and B targets simultaneously from DC and RF power respectively. This machine can deposit the thin films from both thermal evaporation and electron beam induce evaporation techniques. The machine had problems with the high vacuum gauge which was diagnosed and resolved. The PID controller of the machine went bad and malfunctioned. We have diagnosed the problem but could not be fixed. Therefore, we have requested company personnel to restore the factory setting free of cost. The factory reset setting was done online at the company site in Mumbai. We have installed the corrected PID controller back into the machine and now it is fully functional. The additional requirements of the crucibles and thermal boats were limiting the utilization of the machine. Therefore, we have purchased both the accessories. Approximately 35 samples by sputtering and about 110 samples by evaporations have been deposited for different users. The tubular and high-temperature furnaces are in operation and being regularly used by the users.

#### 4.4.5.1 Diagnosis, Repair, and Upgradation of the X-Ray Diffraction System

S.K. Kedia, A. Hussain, F. Singh and A. Tripathi

The XRD system is operational for approximately 17 years in beam hall-2. It was noticed that the crane systems (motor, gearbox, associated wires, and control system) are behaving idiosyncratically. Along with the crane system, we have also faced new problems which include interlock failures and faulty chiller status. Therefore, we have decided to upgrade the machine by repairing/ replacing its components and accessories such as the crane lifting system and chiller. The crane wire was replaced, the gearbox was oiled, new limit switches and interlocks were fixed. The chiller was stopped between the XRD run and shown a faulty status. The chiller was opened, disassembled, components were cleaned, distilled water was replaced, and the chiller system was reset to troubleshoot the new problem. The power unit of the chiller was repaired by AC and chiller group. The frequent power glitches were observed due to faulty MCB in the XRD area. The problem was diagnosed and resolved with the help of the Electrical Group by replacing the new MCB. The water flow to cool the X-ray tube through the mesh filter and slit was choked completely which disabled the X-ray source. The problem was diagnosed with the help of the D8 tool software. The measured water flows in choked conditions and the required water flow to cool the X-ray tube was 1 litre/min and 4 litre/min, respectively. An X-ray tube was opened to clean the filter and fix the issue in-house. The mesh-shaped filter was cleaned using a soft brush and further ultrasonicated for one hour in alcohol. The filter was installed back into the machine. No water leak was observed. Further, an XRD scan has been recorded which is evidence of the offset in the standard peaks of $Al_2O_3$ samples. Therefore, the goniometer alignment was done with the help of a copper and glass slit in the tube scan mode. The facility beamtime run of the five shifts was taken to test the in-situ XRD system and the details analysis of the same is under process. Similarly, the low-temperature XRD setup has also been assembled and tested, the detailed analysis of the same is under process by the user.

## 4.5 RADIATION BIOLOGY

S. A. Khan, A. Sarma, A. Tripathi

The dedicated radiation biology beamline at IUAC houses the ASPIRE [Automated Sample Positioning and Irradiation system for Radiation biology Experiments] system which is utilized for carrying out radiation biology experiments with accelerated heavy ions. In this beamline, cells can be irradiated in air at atmospheric pressure to the preset dose of accelerated heavy ions. The system offers a very good dose uniformity, within 2% standard deviation, over a circular area with diameter of 4 cm. This means that the mean fluence is within 1% of the electronically measured value at the centre of the field. The ion flux uniformity has also been checked by irradiating SSNTD [CN 85]. Six runs were taken in the beamline along with one run for facility test this year.

The dedicated radiation biology laboratory is having the following equipment to facilitate the sample preparation and post irradiation treatments:

(1) Two $CO_2$ incubators, two biosafety cabinets, one small laminar flow bench, two refrigerated centrifuges (Eppendorf's Centrifuge 5430R and Plasto Crafts' Superspin R-V/Fm) and a micro-plate washer (Biotek's ELx50) for cell culture and cell sample preparation.

(2) Analytical equipment like Field Inversion Gel electrophoresis, Normal gel electrophoresis, protein gel electrophoresis set up, Image based cell counter (Countess' Invitrogen) which also gives information about cell viability and Beckman-Coulter Z2 cell counter, PCR machine (Applied Biosystems' Gene Amp PCR System 2400), a crude gel documentation system, UV-Vis Spectrophotometer (Hitachi's U-3300) and an upright Fluorescence microscope (Zeiss Axioplan 2), Perkin Elmer's Victor X5 Multimode Plate Reader.

(3) -20˚C deep freezer, few refrigerators, and LN2 Dewars serve as the storage facilities.

Apart from that, the laboratory section has independent split AC for isolation from the central AC system. Regular work is going on in the laboratory on analytical procedures involving gene expression studies using PCR, Western Blot, Fluorescence Immunostaining studies etc. by the university users.

The following are the projects which are undertaken at present:

1. To optimize the uptake of carbon nanomaterials within the cell and to investigate radio-sensitization as a function of nanomaterial size and dose using therapeutic irradiation with a range of different energies. Monalisa Mukherjee, Amity University, Noida (AUCID 60135)
2. Evaluation of Radio-protective property of 2-4 di nitrophenol in cellular model against particle radiation, Anant Narayan Bhatt, INMAS (AUCID 63105)
3. Chromosomal damage induced by High LET Carbon beam radiation in comparison to gamma radiation in human peripheral blood lymphocytes/ Chinese hamster fibroblast (V79) cells and the effect of Diclofenac sodium in modulating it. Amit Alok, INMAS (AUCID 63106)
4. DNA damage repair kinetics by a potential countermeasure agent using γ-H2AX/comet assay. Paban K Agrawala, INMAS (AUCID 63107)
5. Radio sensitization of human cancer cells using G-quadruplex ligands. Sourav Ghosh, Kalyani University (AUCID 63206)
6. Signalling pathways of activation and secretion of Matrix Metalloproteinases from human lung carcinoma cells after irradiation with carbon ion beam. Payel Dey, Kalyani University (AUCID 63207)
7. Investigation on rapid detection of bacteria using nanoparticles and radiation biology beam lines: A comparative study with low and high linear energy transfer. Balaprasad G. Ankamwar, Savitribai Phule Pune University (AUCID 64322)
8. Ion beam induced mutagenic study of Basmati Rice. Anjali Awasthi, University of Rajasthan (AUCID 66323)
9. Differential cellular response to carbon beam in normal versus transformed cells with special reference to mitochondria. Sweta Sanguri, IUAC (AUCID 67108)
10. Role of autophagy in High Linear Energy Transfer (LET) radiation induced cell death in normal vs. transformed cells. Mitu Lal, IUAC (AUCID 67109)
11. Studies on TLR agonist (mannan) mediated modification in biological radiation response(s) in vitro after carbon beam exposure. Damodar Gupta, INMAS (AUCID 67113)
12. Studies on 2-Deoxy-D-glucose capped Gold-coated Magnetic Nanoparticles ($Au@MFe_2O_4$) for transonic and cancer therapy application. Rajesha Nairy K, P.C. Jabin Science College, Vidyanagar, Hubballi (AUCID 67312)
13. Study of metastatic potential of p53 mutant human lung cancer cells H1299 irradiated with carbon ion. Utpal Ghosh, University of Kalyani (AUCID 70307)

## 4.6 ATOMIC AND MOLECULAR PHYSICS

### 4.6.1 Status of vacuum chamber at $75^0$ beam line in LEIBF

D. K. Swami and C.P. Safvan

Atomic physics related x-ray spectroscopy experiments at low energy are performed in vacuum chamber at $75^0$ beam line in LEIBF. Two silicon drift x-ray detectors (SDD) for x-ray measurements are used in these experiments. The resolution of these detectors are ~150 eV at 5.9 keV. Two Silicon surface barrier detectors are also used for measurements of scattered and back scattered charged particles. At a time, 4-5 targets can be used. For the linear and angular motion of the targets, one linear motion feed through and one rotatable axis-360° adjustable stage are mount at the top of the lid respectively. In this chamber, one collimator (penetrable faraday cup) was installed and aligned at the entrance of the ion beam before the targets. During experiments, vacuum inside the chamber is $10^{-6}$-$10^{-7}$ mbar. This year, for atomic physics experiments in LEIBF, Data Acquisition System (DAQ) was also upgraded from CAMAC DAQ to VME based DAQ.

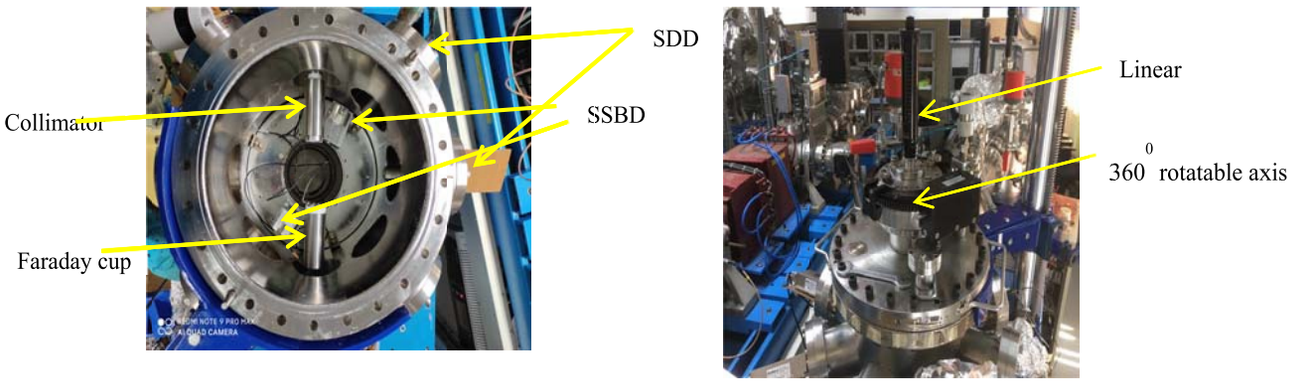


Fig. 1: Schematic of vacuum chamber at $75^0$ beam line in LEIBF.

### 4.6.2 Status of general purpose atomic physics vacuum chamber (GPAC) at beam hall-II

D. K. Swami and C.P. Safvan

Highly charged ion beam solid collision x-ray spectroscopy experiments at high energy are performed in general purpose atomic physics vacuum chamber (GPAC) at beam hall-II. Two silicon drift x-ray detectors (SDD) for x-ray measurements are used in these experiments. These SDDs detectors are install at different angles with respect to ion beam. The experimental resolution of these detectors are ~150 eV at 5.9 keV. Two Silicon surface barrier detectors are also used for measurements of scattered and back scattered charged particles. . At a time, 12 targets can be used. During experiments, vacuum inside the chamber is $10^{-6}$ - $10^{-7}$ mbar. This year, for atomic physics experiments in Beam hall-II, Data Acquisition System (DAQ) was also upgraded from CAMAC DAQ to VME based DAQ. It was tested with radioactive source as well as an ion beam also. It is working properly.

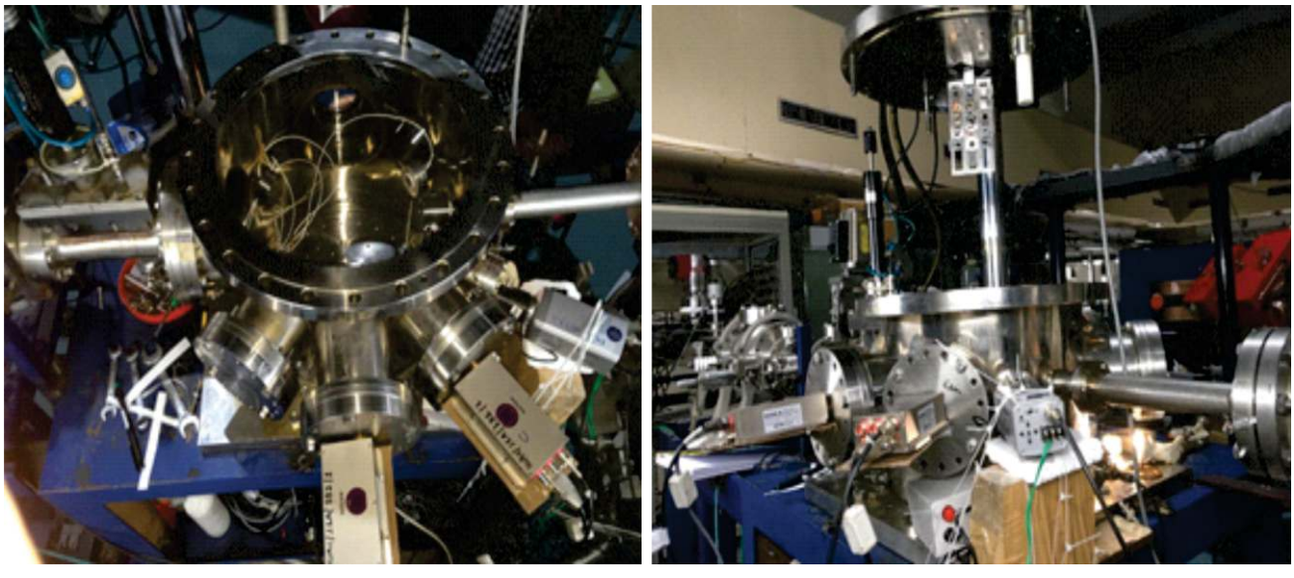

Fig.2: Schematic of GPAC in beam hall-II.

### 4.6.3 Status of Electro Static Analyzer (ESA) for post foil charge state measurements at beam hall-II

D. K. Swami and Dr. C.P. Safvan

Inter University Accelerator Centre, Aruna Asaf Ali Marg, New Delhi-110067, India.

Knowledge of post foil charge state distributions is always useful in selecting the beam energy for a particular charge state of interest with maximum yield. For studying the charge state fraction in post foil, we are in the process of developing a new technique involving an Inclined and Straight Plate Electrostatic Analyzer (ISESA) in which one plate is held parallel and the other kept inclined at a certain angle relative to the beam axis in beam hall-2. Therefore an ISESA is asymmetric about the beam axis. It is essential to apply the voltages to the plates in such a manner that the beam is deflected towards the inclined one. A small gap (10mm) between the plates at the entry causes large deflections due to a high field. As the ions move forward, the gap increases (causing a lower field) so that the ions can escape without hitting the plate. This inclination of one deflecting plate allows better resolution of charge states and increases the number of charge states escaping without hitting the plate also.

The setup has been installed at the back of the General Purpose Vacuum Chamber for atomic physics experiment in the beam line as shown in figure 1. A gate valve placed in between the chamber and ISESA allows us to isolate the chamber and ISESA during the experiment. Two beam collimating slit systems are placed to align the beam with the axis of in the ISESA. ISESA is being used to deflect the post foil charge state so that deflected ions in the field region does not hit the plate at the exit. A trapper drift tube chamber of 1.5 m long is used so as to transfer ions tangentially after passing the ISESA. Trapper drift tube chamber provides opportunity to place a 220 mm long Position Sensitive Proportional Counter (PSPC). A P-10 gas filled Position Sensitive Proportional Counter is used to measuring the position of different charge states simultaneously. There is one Faraday cup placed at the end of Trapper drift tube chamber is used to monitor the beam current throughout the experiment. A vacuum control system has been designed to create high vacuum inside the trapper drift chamber and ISESA. To achieve the desired vacuum, one turbo pump (300 l/sec) is employed on the trapper drift tube chamber. To measure the vacuum inside the ISESA, a Pirani gauge and a full range cold cathode gauge are used.

This year, a facility test of electro static analyzer with ion beam was performed. In this experiment, Ni ion beam with different energy was bombarded on C. Two silicon drift x-ray detectors (SDD) for x-ray measurements were used in this experiment. One position sensitive proportional counter was also used for post foil charge state measurement. This facility test was successfully done. Data from X-ray and charged particle detectors with VME based DAQ were recorded. In this facility test, we found ESA, all detectors and electronics were working properly. Recorded data are being analyzed.

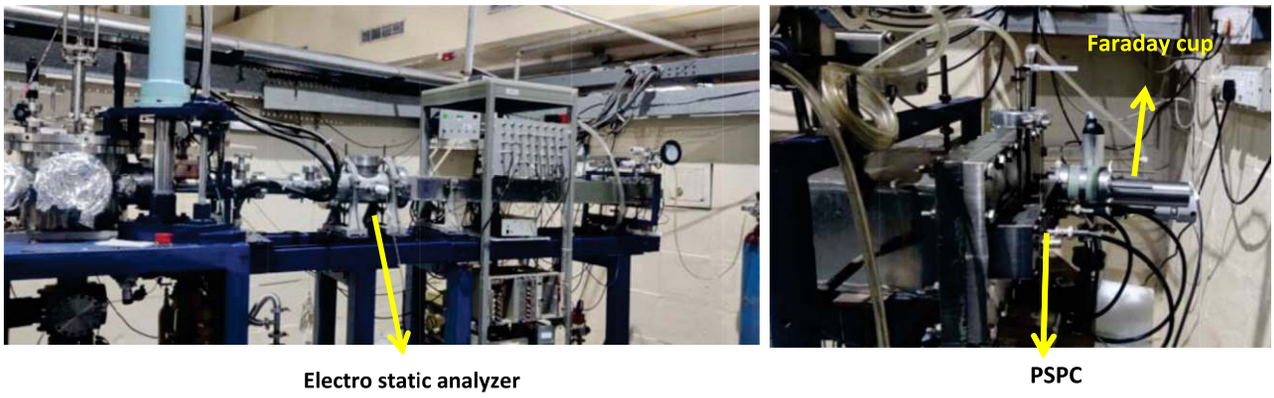


Fig.3: Schematic of Electro Static Analyzer in beam hall-II.